A virtual reactor for simulation of plasma enhanced chemical vapor deposition

Krzhizhanovskaya, V.

Chapter 2. Modeling and Simulation Part I: 1D Flow and 1D Plasma Discharge*

2.1. Introduction

In this chapter, our goal is to develop a simplified model allowing one to describe the processes in a PECVD reactor and to predict some of the parameters measured in experiments. We are aware that a 1D model can give only limited agreement and trends. More accurate simulations are to come from 2D and 3D expanded models which are introduced in the subsequent chapters.

One of the most widespread methods of growing hydrogenated amorphous silicon films is the technology based on deposition from the gas phase of silicon-containing radicals produced by the decomposition of silane by RF discharge plasma in PECVD reactors. At present, various types of such systems are used. In one of these, the diode system, the substrate serves as one of the electrodes (see Fig. 1.1). In another system, belonging to a widely used class of systems with remote plasma and usually called a triode system, the substrate is placed outside the plasma discharge zone (see Fig. 2.1 and Section 2.7.7). This triode system offers the advantage of sheltering the substrate from ion bombardment, which can impair the surface quality. It was proposed and thoroughly investigated in [1]. By increasing the growth rate and film quality through optimizing the parameters of PECVD reactors, significant technological advantages can be attained. Therefore, various models are being proposed, which, with differing degrees of detail, describe the processes in the growth chamber and allow improvements to be made in the reactor design.

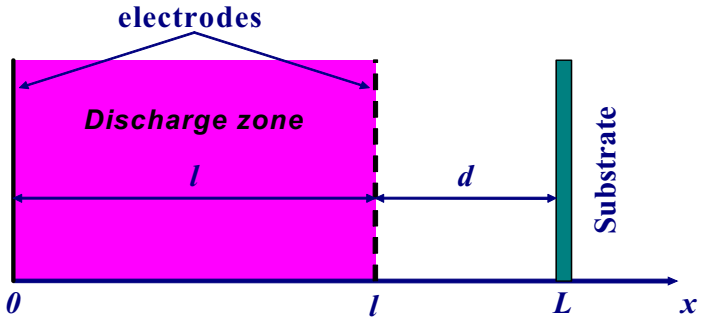

Fig. 2.1. Triode configuration and notations.

* Parts of this chapter were published in [12-15]

The first comprehensive model of the growth process of hydrogenated amorphous silicon film was proposed in [2].

A rather simple and effective model developed later [3] is suitable for making prompt estimates of all basic process parameters with sufficient accuracy. Apart from silane (SiH_4), 12 major chemical components of the mixture are included in this model: SiH_n , n = 1–3; H; H_2 ; Si_2H_n , n = 3–6; Si_3H_8 ; Si_2H_6* ; and Si_2H_6** (asterisks denote the excited electronic state). Recently, a similar model but with a different set of chemical components and a much more elaborate presentation of the electronic subsystem was proposed [4]. The authors carried out quite detailed measurements of the system parameters and provided the experimental data necessary for verifying the models.

In the framework of the model proposed in [3], the authors carried out a computational study of the physical and chemical processes occurring in the pure silane plasma in a diode reactor and performed a detailed analysis of the role of various components and the effect of the system parameters on film growth for major operating regimes. It was found that at low pressures molecular hydrogen accumulates in the chamber, so that silane ceases to be the only carrier component. In addition, a technology based on diluting silane with hydrogen is often used in practical applications, which saves silane and makes the production of silicon films ecologically cleaner. Under these conditions, the model of [3] is inadequate.

In this study, a model that takes into account the changes in silane concentration during film growth is presented. Transport due to diffusion was simulated using, instead of fixed coefficients, those calculated by Wilke's formula representing a first approximation of diffusion in a multicomponent medium. It has been shown that further elaboration of the description of diffusion processes does not improve the accuracy of the calculations of the component fluxes onto the film surface. Simuations of the plasma discharge were carried out using a fluid model [5] providing a means to calculate the electron densities.

Throughout this thesis, a modeling approach is used where the complete simulation domain is subdivided into two parts: the discharge zone, where the plasma processes should be properly simulated, and the rest of the reactor volume, where only chemical reactions and transport processes should be computed (see also Section 1.2.1 and Fig. 1.1). This subdivision is justified by the fact that the electron energy experiences a very rapid exponential decrease outside the discharge, therefore electrons do not cause dissociation there. In addition, electron-ion recombination eliminates the charged particles already at a very short distance from the plasma discharge zone, therefore only the neutrals shall be considered there [12,16,17]. This effect will be illustrated in Section 4.3 where the results of 2D plasma simulation are presented. In the discharge volume, a combined kinetic-fluid plasma model is used (described in the next Section), and in the whole reactor volume a gas dynamic approach is used for the reactive flow simulation (described in Section 2.3). The plasma simulation provides the reactive flow code with the electron density distribution averaged over one RF cycle, while the plasma model uses the background gases concentrations provided by the flow code. The process of data exchange is organized iteratively, and proceeds until the background gas concentration does not change any longer.

This approach is not entirely self-consistent. Ideally, one should simulate plasma and flow with full coupling, solving the whole set of plasma and flow equations together. However, that would be computationally prohibitive because of the large gap in scales (several orders of magnitude) between the required time steps for plasma and flow. Other limitations of this approach are the following: it is assumed that ions do not contribute to the film growth (which can add about 10%), and all the electrons inside the discharge zone are assumed to have sufficient energy to cause dissociation.

In this Chapter, expressions for the rate constants of reactions initiated by electron impact in silane-hydrogen mixtures have been derived. Hence, the processes in reactors could be studied for a wider range of parameters, and the processes taking place in silane diluted with molecular hydrogen could be simulated. The proposed model describes the processes in triode-type reactors with the discharge zone moved away from the substrate. Finally, in this work, the effect of the reactor volume, which in almost every real installation does not coincide with the discharge zone, has been accounted for in a correct manner.

2.2. 1D plasma model

Direct Monte Carlo simulation of electron kinetics showed that at pressures higher than 0.1 Torr we can use a gas-dynamic approach for electron and ion description. In the present work we used a 1D fluid model [5] for simulation of the RF discharge processes. The continuity equations for electrons, ions and neutrals are solved consistently with the balance equation for the average electron energy, and with the Poisson equation for the electric field distribution. The model accounts for the emission and action of secondary electrons produced by the primary electron impact on the surface of the electrode.

The rates of inelastic electron collisions and the electron transport coefficients are calculated by solving the Boltzmann equation for the electron energy distribution function (EEDF) f_0 in the two-term approximation: [5]

$$-\frac{\partial}{\partial\varepsilon}\left(\frac{2e^2E^2\varepsilon}{3mN\sigma_t}\frac{\partial f_0}{\partial\varepsilon}\right)=St\{f_0\} \tag{2.1}$$

Here, ε is electron energy, N is neutral gas number density, E is electric field, σ_t is scattering cross-section, m is electron mass, and collision term $St\{f_0\}$ includes only inelastic electron-ion collisions.

The EEDF is calculated as a function of the electric field for a given composition of the neutral background density. A look-up table is then constructed to obtain the collision rates and electron transport coefficients used in the fluid model as functions of the average electron energy.

While calculating the EEDF, the electric field was assumed to be spatially uniform and constant in time. This approximation was compensated for in the fluid model by the spatial and temporal variation of the averaged electron energy.

Further details on this RF discharge model have been published in [5], including the list of all chemical reactions simulated in the plasma discharge volume (ionization, dissociation, excitation, recombination, attachment).

Within the fluid model, we solve the continuity and average electron energy equations for electrons (denoted with subscript *e*), and continuity and momentum equations for positive and negative ions (denoted with *p* and *n* subscripts):

$$\begin{cases} \dfrac{\partial N_e}{\partial t} - \dfrac{\partial\left(\mu_e E N_e + \partial\left(D_e N_e\right)/\partial x\right)}{\partial x} = \left(\nu_i - \nu_a\right) N_e + \nu_d N_n - \nu_b N_e N_p \\ \dfrac{\partial N_e U_e}{\partial t} - \dfrac{\partial\left(\mu_u E N_e U_e + \partial\left(D_u N_e U_e\right)/\partial x\right)}{\partial x} = eE\left(\mu_e E N_e + \dfrac{\partial D_e N_e}{\partial x}\right) - \nu_u N_e U_e \end{cases} \tag{2.2}$$

$$\begin{cases} \dfrac{\partial V_p}{\partial t} + \dfrac{\partial V_p^2/2}{\partial x} = \dfrac{eE}{M_p} - W_p N V_p \\ \dfrac{\partial V_n}{\partial t} + \dfrac{\partial V_n^2/2}{\partial x} = \dfrac{-eE}{M_n} - W_n N V_n \end{cases} \tag{2.3}$$

$$\begin{cases} \dfrac{\partial N_p}{\partial t} + \dfrac{\partial N_p V_p}{\partial x} = \nu_i N N_e - \nu_b N_e N_p - \beta N_p N_n \\ \dfrac{\partial N_n}{\partial t} + \dfrac{\partial N_n V_n}{\partial x} = \nu_a N N_e - \nu_d N_n - \beta N_p N_n \end{cases} \tag{2.4}$$

Here t is time, x is position along axis X perpendicular to the electrodes, V_n, V_p are velocities of negative and positive ions; M_n, M_p, W_n, W_p are masses and frequencies of ions scattering; β is ion-ion recombination rate; e is elementary charge; E is electric field; N, N_e, N_n, N_p are number densities of neutrals, electrons, negative and positive ions; ν_i, ν_a, ν_d, ν_u are frequencies of ionization, attachment, detachment and inelastic collisions of electrons; μ_e, D_e are electron mobility and diffusion transport coefficients; μ_u, D_u are mobility and diffusion coefficients for the average electron energy U_e; and ν_b is electron-ion recombination rate.

The set of equations (2.2-2.4) are solved consistently with the Poisson equation for the potential Φ:

$$\frac{d^2\Phi}{dx^2} = 4\pi e\left(N_e + N_n - N_p\right), \quad E = -\frac{d\Phi}{dx}. \tag{2.5}$$

The secondary electrons, also called γ-electrons, emitted from the electrode surface can gain very high energy (of order of plasma potential, 10-100 eV), and thus can initiate a number of ionization actions. The usual gas-dynamic approach does not take that into account, but averages the electron energy over all electrons (most of them have an energy of order of electron temperature, about 1-3 eV). Therefore the second type of electrons needs to be introduced, for which we solve equations (2.2) separately.

Boundary conditions take into account ion-electron emission:

$$\begin{cases} \dfrac{N_e V_t}{4} - \mu_e E N_e - \dfrac{\partial D_e N_e}{\partial x} = k_{em} N_p V_p \\ \dfrac{N_e V_t U_e}{4} - \mu_u E N_e U_e - \dfrac{\partial D_u N_e U_e}{\partial x} = k_{em} N_p V_p U_e \end{cases} \tag{2.6}$$

Here V_t denotes thermal velocity of electrons and k_{em} ion-electron emission coefficient.

To account for gas heating, a heat transfer equation was solved:

$$\frac{d\lambda(dT/dx)}{dx} = Q \tag{2.7}$$

with λ, thermal conductivity coefficient; Q, the Joule heating due to ion and electron energy loss and T, gas temperature.

The pressure $p = NkT$ is set constant.

The data on chemistry, kinetic coefficients, cross-sections and other model details can be found in [5].

Special attention was paid to resolving the sheaths, an important zone within the discharge volume where the electric field and other plasma parameters, like electron and ion concentration and energies, are different from those in the bulk. To resolve the sheath, the computational mesh was manually refined near the electrode walls.

Validation and extensive testing of the model described above has been performed earlier [5]. The main plasma parameters predicted by simulations were found to be in good agreement with experimental data. We additionally validated the model in the parameter range used in our numerical experiments, and later compared the results of our simulations with those calculated by another 1D model developed in the group of Prof. Goedheer [4]. The electron concentration profiles (spatial distribution between the electrodes) produced by the two models slightly differed in the sheath width (see Fig. 2.2), however the net effects (the mean electron concentration and the film growth parameters) simulated with two models were reasonably close to each other.

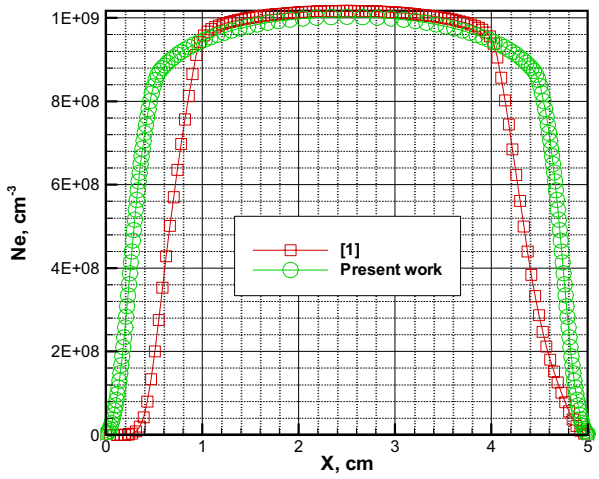

Fig. 2.2. Comparison of electron distribution predicted by the two models. p=0.15Torr, W=0.0366 W/cm^2. In the figure, [1] indicates the result predicted by the 1D model developed in the group of Prof. Goedheer [4].

2.3. 1D reactive flow dynamics model

In the proposed model of a PECVD reactor, the gas-phase processes in the chamber are described by one-dimensional equations of chemical kinetics, in which, as estimated in [3], only the diffusion transfer processes are taken into account:

$$\frac{\partial n_i}{\partial t} = \frac{\partial}{\partial x}\left(D_i \frac{\partial n_i}{\partial x} \right) + F_i \,. \tag{2.8}$$

Here, n_i is the number density of the i-th component and F_i is the source term due to chemical reactions (more details can be found in [3]). The effective diffusion coefficient of the i-th component D_i is calculated by Wilke's formula [6], commonly used in practical calculations of multicomponent gas mixtures:

$$D_i = (n - n_i) \Big/ \sum_{k=1,k\neq i}^{Nk} \frac{n_k}{D_{ki}} \text{, cm}^2\text{/s} \tag{2.9}$$

where n is the total number density of the mixture.

The binary diffusion coefficient D_{ki} is calculated by the formula of the molecular kinetic theory of gases [7] with use of the Lennard-Jones 6-12 potential:

$$D_{ki} = 0.002628 \cdot \frac{\sqrt{T^3/2\mu_{ki}}}{p\sigma_{ki}^2 \Omega_{ki}^{(1.1)*}\left(T_{ki}^*\right)} \text{, cm}^2\text{/s} \tag{2.10}$$

Here, $\mu_{ki} = m_k m_i/(m_k + m_i)$ is the effective mass of the kth and ith species, m_i is the molecular weight of the ith species, $\sigma_{ki}=(\sigma_k+\sigma_i)/2$ is the effective collision diameter, $T_{ki}^* = kT/\varepsilon_{ki}$ is the characteristic temperature, $\varepsilon_{ki} = (\varepsilon_k \varepsilon_i)^{1/2}$ is a parameter of the potential for intermolecular interaction (potential well depth), k is the Boltzmann constant, and $\Omega_{ki}^{(1.1)*}(T_{ki}^*)$ is a reduced Ω-integral of collisions for mass transfer normalized by the Ω-integral of the model of hard spheres. Values of the T_{ki}^* function for a wide range of characteristic temperatures T_{ki}^* can be found in monograph [7]; in the calculations, approximate formulas given in [8] were used. Values of the Lennard–Jones potential parameters σ_i and ε_i borrowed from [9] are given in Table 2-1.

Table 2-1. Parameters of the Lennard–Jones potential

Component	σ_i, Å	ε_i/k, K
SiH_4	4.084	207.6
SiH_3	3.943	170.3
SiH_2	3.803	133.1
SiH	3.662	95.8
H	2.5	30.0
H_2	2.915	59.7
Si_2H_6	4.828	301.3

Component	σ_i, Å	ε_i/k, K
$Si_2H_6^*$	4.828	301.3
$Si_2H_6^{**}$	4.828	301.3
Si_2H_5	4.717	306.9
Si_2H_4	4.601	312.6
Si_2H_3	4.494	318.2
Si_3H_8	5.562	331.2

In [10], experimental determinations of the ambipolar diffusion coefficients of silyl in silane and molecular hydrogen were carried out and found to be equal to 140±30 and 580±140 cm^2/s, respectively, at the temperature 320 K and pressure 1 Torr. Under these

conditions, formula (2.10) gives the values of 111 and 536 cm^2/s, respectively, which is in good agreement with the measured data.

In the next section we describe the boundary conditions that take into account the deposition process.

2.4. Modeling chemical processes and deposition

2.4.1. Model of the deposition process

To model the deposition process, a new model of sticking probabilities was developed [12]. In this model only neutral radicals having free bonds contribute to the film growth (Si_nH_m for *m=2n-1, m=2n, m=2n+1, n≥1*). Neither detachment nor ion bombardment is considered, which potentially can influence the deposition process and film properties and should be included in the model in the future, as was done in [18]. There is a possibility to further improve the model by refining the experimental data that allowed estimating the sticking probabilities; yet a better way would be to develop an atomic-level model for simulation of heterogeneous reactions on the surface. The latter approach is something for the future, since it will definitely require extensive experimental and theoretical developments.

To implement the deposition model, a boundary condition with a concentration jump near the surface was introduced. The complete model of surface processes is based on a simplified kinetic theory which allowed us to derive the boundary conditions for the species concentration jump [3]:

$$-D_i \frac{\partial n_i}{\partial x} = \frac{s_i c_i}{2(2-s_i)} n_i \tag{2.11}$$

Here, $\partial/\partial x$ is a normal derivative at the outside of the surface, $c_i = 2\sqrt{2kT/\pi m_i}$ is the thermal velocity, and s_i is the sticking probability of the *i*-th species. Sticking probabilities are chosen as follows [2,3]: $s_i = 0$ for Si_nH_{2n+2} (no free bonds), $s_i = 0.15$ for Si_nH_{2n+1} (1 free bond), $s_i = 1$ for Si_nH_{2n}, Si_nH_{2n-1} (2 free bonds). In [3] it was shown that the actual values of the sticking coefficients s_i do not significantly influence the deposition rate.

The deposition rate is calculated as follows:

$$R = -v_{Si} \sum_{i=1}^{N} q_i D_i \frac{\partial n_i}{\partial x}, \tag{2.12}$$

where $v_{Si} = 2.195 \cdot 10^{-29}\ m^3$ is the silicon atom volume, and q_i is the number of silicon atoms in a depositing radical.

In this simplified model, we did not consider surface reactions leading to hydrogen release from the surface, which should be taken into account for accurate predictions of the film composition. We shall note however that this omission will not affect the net growth rate (calculated from the silicon atom contents), thus the model is well suitable for the film deposition rate estimations. Hydrogen concentration in the film can be corrected within our approach by comparing the simulation results with experimental data and finding reaction rate constants of the missing surface reactions. This procedure will require a large collection of experimental data in a complete range of process conditions, and a separate

research that will allow identifying the most essential surface process and their rate constants. This will be one of the directions of future work.

2.4.2. Chemical components and reactions

Apart from silane (SiH_4) and diluent hydrogen (H_2), 12 contributing radicals are included in this model: H, SiH_n , n = 1–3; Si_2H_n , n = 3–6; Si_3H_8 ; $Si_2H_6^*$; and $Si_2H_6^{**}$ (asterisks denote the excited electronic state).

Chemical reactions considered essential for adequate modeling are listed in **Table 2-2**. In addition, silane and disilane pyrolysis reactions are taken into consideration, which, as is indicated by the simulations, give an insignificant contribution to the total chemical balance.

Table 2-2. List of chemical reactions and reaction constants used in this Chapter.

N^o	Reactions	Reference rate constants, cm^3/s
R1	$SiH_4 + e \rightarrow SiH_3 + H + e$	$3.000 \cdot 10^{-11}$
R2	$SiH_4 + e \rightarrow SiH_2 + 2H + e$	$1.500 \cdot 10^{-10}$
R3	$SiH_4 + e \rightarrow SiH + H + H_2 + e$	$9.340 \cdot 10^{-12}$
R4	$SiH_4 + e \rightarrow SiH_2 + H_2 + e$	$7.190 \cdot 10^{-12}$
R5	$H_2 + e \rightarrow 2H + e$	$4.490 \cdot 10^{-12}$
R6	$Si_2H_6 + e \rightarrow SiH_4 + SiH_2 + e$	$3.720 \cdot 10^{-10}$
R7	$Si_2H_6 + e \rightarrow Si_2H_4 + H_2 + e$	$3.700 \cdot 10^{-11}$
R8	$SiH_4 + H \rightarrow SiH_3 + H_2$	$2.530 \cdot 10^{-12}$
R9	$SiH_4 + SiH_2 \rightarrow Si_2H_6^*$	$1.000 \cdot 10^{-11}$
R10	$SiH_4 + SiH \rightarrow Si_2H_3 + H_2$	$1.700 \cdot 10^{-12}$
R11	$SiH_4 + SiH \rightarrow Si_2H_5$	$2.500 \cdot 10^{-12}$
R12	$SiH_4 + Si_2H_5 \rightarrow SiH_3 + Si_2H_6$	$5.000 \cdot 10^{-13}$
R13	$SiH_4 + Si_2H_4 \rightarrow Si_3H_8$	$1.000 \cdot 10^{-10}$
R14	$SiH_3 + H \rightarrow SiH_2 + H_2$	$1.000 \cdot 10^{-10}$
R15	$SiH_3 + SiH_3 \rightarrow SiH_4 + SiH_2$	$1.500 \cdot 10^{-10}$
R16	$SiH_3 + SiH_3 \rightarrow Si_2H_6^{**}$	$1.000 \cdot 10^{-11}$
R17	$SiH_3 + Si_2H_5 \rightarrow SiH_4 + Si_2H_4$	$1.000 \cdot 10^{-10}$
R18	$SiH_3 + Si_2H_5 \rightarrow Si_3H_8$	$1.000 \cdot 10^{-11}$
R19	$SiH_3 + Si_2H_6 \rightarrow SiH_4 + Si_2H_5$	$3.270 \cdot 10^{-12}$
R20	$SiH_2 + H \rightarrow SiH + H_2$	$7.960 \cdot 10^{-13}$
R21	$SiH_2 + Si_2H_6 \rightarrow Si_3H_8$	$1.200 \cdot 10^{-10}$
R22	$Si_2H_3 + H_2 \rightarrow Si_2H_5$	$1.700 \cdot 10^{-12}$
R23	$Si_2H_4 + H_2 \rightarrow SiH_4 + SiH_2$	$1.000 \cdot 10^{-10}$
R24	$Si_2H_5 + H \rightarrow Si_2H_4 + H_2$	$1.000 \cdot 10^{-10}$
R25	$Si_2H_6 + H \rightarrow SiH_4 + SiH_3$	$7.160 \cdot 10^{-12}$
R26	$Si_2H_6 + H \rightarrow Si_2H_5 + H_2$	$1.430 \cdot 10^{-11}$
R27	$Si_2H_6^* \rightarrow Si_2H_4 + H_2$	$5.000 \cdot 10^{6}$ s^{-1}

R28	$Si_2H_6^* + M \rightarrow Si_2H_6 + M$ (M – any particle colliding with $Si_2H_6^*$)	$1.000 \cdot 10^{-10}$
R29	$Si_2H_6^{**} \rightarrow SiH_4 + SiH_2$	$2.300 \cdot 10^{7}$ s^{-1}
R30	$Si_2H_6^{**} \rightarrow Si_2H_4 + H_2$	$2.300 \cdot 10^{7}$ s^{-1}
R31	$Si_3H_8 + H \rightarrow Si_2H_5 + SiH_4$	$2.170 \cdot 10^{-11}$
R32	$Si_3H_8 + SiH_3 \rightarrow Si_4H_9 + H_2$	$1.000 \cdot 10^{-11}$

Data are given for the inter-electrode separation l^0 = 2.5 cm, partial pressures of molecular hydrogen and silane p^0 = 0.125 Torr, temperature T^0 = 520 K, and discharge power W^0 = 0.25 mW/cm^3.

2.4.3. Electron impact reaction rate constants

The approach used for calculating the electron-induced reaction rates, avoiding calculation of the corresponding electron temperatures, was proposed in [3] for pure silane plasmas and extended for diluted silane mixtures in [12]. This approximate method for determining the dependencies of the constants of electron-impact processes on the discharge parameters was based on a number of assumptions: the concentration of the background gasses (SiH_4 and H_2) was assumed to be much higher than the concentration of other species; the electron temperature was assumed to be sufficiently small compared to the ionization threshold; the plasma was considered quasi-neutral and the recombination losses small compared to the diffusion losses. The electron energy distribution function was modeled in the Boltzmann form, taking into account that the electron temperature corresponds to the high-energy "tail" of the electron distribution and depends on the pressure of the gas and the inter-electrode spacing. The parameterization formula obtained in [10] is applicable to the relatively low power discharges, where the contribution of the high-energy γ-electrons into ionization can be neglected. The applicability of this formula for high-power discharges remains to be validated against a comprehensive plasma simulation. The processes neglected while deriving this relationship (electron-ion recombination and γ-electrons emission) are properly taken into account in the plasma discharge model.

To define the dependence of the electron-induced reaction rate constants on partial pressures and the inter-electrode separation l, the following relationship between the reaction constants k_r and the ionization constants k_i was used [3]:

$$k_r / k_r^0 = \left(k_i / k_i^0\right)^{\varepsilon_r/\varepsilon_i} \tag{2.13}$$

where $\varepsilon_r, \varepsilon_i$ are the thresholds for the chemical reaction and ionization, respectively [11], and the superscript "0" refers to the reference conditions for which the values of the constants are known (see **Table** 2-2).

Then, assuming that the plasma as a whole is neutral, that the removal rate of electrons is equal to that of ions (mainly SiH_2^+ ions), and that the carrier mixture consists of silane and molecular hydrogen, the following expression can be obtained using formula (2.9):

$$\frac{k_i}{k_i^0} = \frac{n}{n^0}\frac{n^0_{SiH_4}}{n_{SiH_4}}\frac{\left(n^0_{SiH_4}/D^0_{SiH_4SiH_2} + n^0_{H_2}/D^0_{H_2SiH_2}\right)}{\left(n_{SiH_4}/D_{SiH_4SiH_2} + n_{H_2}/D_{H_2SiH_2}\right)}\left(\frac{l^0}{l}\right)^2 \tag{2.14}$$

Here, n and n^0 are the number densities of the species under present and reference conditions respectively, D_{ij} is the binary diffusion coefficient. For the reference conditions, a silane–hydrogen mixture is chosen with partial pressures of hydrogen and silane $p^0_{H_2} = p^0_{SiH_4} = 0.125$ Torr at the temperature $T^0 = 520$ K and the inter-electrode distance $l^0 = 2.5$ cm, because the constants for these conditions were determined in [2].

Comparison of the electron-induced reaction rate constants calculated with the expression (2.13)-(2.14) with those calculated from EEDF showed a good agreement in the parameter range used in our simulations.

2.5. Numerical methods, implementation and computational environment

2.5.1. Numerical methods and algorithms

The mathematical model describing the diffusion processes in a chemically reacting mixture is represented by a stiff system of nonlinear equations. For solving this system of equations (2.8), a numerical method that takes into account the specific features of these equations was developed [3]. The source terms F_i can be rewritten in the form of $F_i = f_i - A_i n_i$, with $f_i \geq 0$ being the chemical production rate of the ith species, $\partial f_i / \partial n_i = 0$, and $A_i \geq 0$ is the depletion rate. Then the following implicit numerical scheme can be used for each species:

$$\left(1 + \Delta t\, A_i^k\right) n_i^{k+1} - \Delta t\, D_i n_{i_{xx}}^{k+1} = n_i^k + \Delta t\, f_i^k, \tag{2.15}$$

where Δt is the time step value, superscript k is time step index, and $n_{i_{xx}}^{k+1}$ is the second spatial derivative of the i-th species concentration. Each time step, the system (2.15) is solved by the sweep-time algorithm. This approximation ensures a positive unconditional convergence of the algorithm for any value of the time step. An automatic time step selection procedure was used, based on controlling the maximal changes of relative concentrations per one time step. Extensive testing of the scheme showed that it allows to obtain stable convergence for $\Delta t >> \Delta t_{chem.}$, where Δt_{chem} is the characteristic time of the fastest chemical reaction. The simulation proceeds for the time τ during which the complete volume of the gas in the chamber will be fully replaced by the fresh gas supplied through the inlet: $\tau = M_0/Q$, where M_0 is the total mass of the gas in the chamber and Q is mass inflow rate. In real-life reactor chambers this characteristic "forced convection" time is much longer than the characteristic time of diffusion and chemical reactions, therefore within the time τ the system will arrive at a quasi steady state.

2.5.2. Implementation and computational environment components

The plasma and the 1D reactive flow models were implemented as FORTRAN computer codes. The coupling between the codes described in Section 2.1 consists in exchanging data files that contain the variable distributions. The codes are platform-independent and were compiled and used on Unix-like and Windows operating systems with the open-source GNU FORTRAN compilers. To facilitate the problem formulation and parameter setting procedure, as well as to organize parameter sweep simulations, a computational environment called REAF was developed, which served as a prototype of the Virtual Reactor environment developed and extended later [20].

2.6. Analytical results

With some assumptions it is possible to solve equations (2.8) analytically. That will allow fast estimation of tendencies and provide a fairly rigorous check of our numerical simulations for some test cases. Asymptotic analysis based on the difference in scale of various processes led to the analytical formulas explaining the influence of the chamber conditions on the deposition process. In [3], such relationships were derived for the diode system, and in this work, they were expanded for the triode configuration (see Fig. 2.1). The entire simulation domain of $0<x<L$ was divided into two subdomains: $0<x<l$, where the density n_e of electrons initiating the chemical reactions was taken equal to that in the inter-electrode gap, and $l<x<L$, where the electron energy is not sufficient to initiate chemical reactions, thus can be set to zero (see also explanations in section 1.2.1). It is assumed that in the latter zone of size $d=L–l$, only monomolecular reactions or reactions involving molecular collisions are taking place.

Estimates of basic processes similar to those in [3] produced the following simplified equation for the behavior of silyl, the main species contributing to the film growth:

$$D_{SiH_3}\, d^2 n_{SiH_3} \big/ dx^2 = 2k_8 n_H n_{SiH_4} - k_{32} n_{SiH_3} n_{Si_3H_8}\,, \tag{2.16}$$

where k_i is the constant of the i-th reaction (i is the reaction number in Table 2-2). The boundary condition (2.11) with a sticking coefficient $s_{SiH3}= 0.15$ is used.

A corresponding analysis for atomic hydrogen, which is the major initiator of silyl production, leads to the following balance equation in the discharge zone $0<x<l$:

$$-D_H\, d^2 n_H \big/ dx^2 = 2k_2 n_e n_{SiH_4} - k_8 n_{SiH_4} n_H\,. \tag{2.17}$$

Outside the discharge zone at $l<x<L$ the behavior of atomic hydrogen is described by the same equation, except that the first term on the right-hand side should be omitted ($n_e = 0$), which means that hydrogen escapes the discharge zone only through diffusion. Solving these equations with boundary conditions (2.11) in the absence of deposition ($s_H = 0$) and with the condition of continuity of solutions at the boundary between the zones (at $x=l$), we obtain an analytical expression for the atomic hydrogen concentration profile:

$$n_H = \frac{2k_2 n_e}{k_8}\left(1 - \frac{\sinh\left(d/L_H\right)}{\sinh\left(L/L_H\right)}\right)\cosh\frac{x}{L_H},\ 0 < x < 1\,, \tag{2.18}$$

$$n_H = \frac{2k_2 n_e}{k_8} \frac{\sinh\left(l/L_H\right)}{\sinh\left(L/L_H\right)} \cosh\frac{L-x}{L_H},\ l < x < L\ . \tag{2.19}$$

Substitution of expressions (2.18) and (2.19) into equation (2.16) yields an analytical expression for the flux of silyl towards the surface as a function of the system parameters:

$$\Gamma_{SiH_3} = \frac{2k_2 n_e n_{SiH_4} L_3}{\sinh\left(L/L_3\right)} \left[\begin{array}{l} 2\sinh^2\frac{l}{2L_3} + \frac{L_H^2}{L_3^2 - L_H^2} \frac{1}{\sinh\left(L/L_H\right)} \times \\ \left(\cosh\frac{l}{L_3}\sinh\frac{L}{L_H} - \cosh\frac{L}{L_3}\sinh\frac{l}{L_H} - \sinh\frac{d}{L_H} \right) \end{array} \right] \tag{2.20}$$

$$L_H = \sqrt{D_H/(k_8 n_{SiH_4})}\ ,\ L_3 = \sqrt{D_{SiH_3}/\left(k_{32} n_{Si_3H_8}\right)}. \tag{2.21}$$

Here, L_H and L_3 are reaction-limited diffusion lengths for atomic hydrogen and silyl, respectively, introduced in [3] and defined as the distance which a diffusing species will travel before undergoing transformation in chemical reaction. More details on diffusion-reaction lengths and their analysis for different species will be given in Section 2.7.8. For $l \to L$ ($d \to 0$), expressions (2.18)-(2.20) describe a diode system.

To conclude this section, we consider the behavior of silylyl. In the discharge zone, silylyl is produced mainly via the dissociation of silane by electron impact, reaction R2 in Table 2-2, and through recombination reaction R23, whereas, outside this zone, it is produced in recombination reaction R15 and, again, R23. Chemical removal of silylyl in both cases depends on its addition reaction with silane (R9). The Si_2H_4 radical is an intermediate product of the cycle of fast chemical reactions R9, R27, and R23; therefore its concentration is close to the equilibrium value $n^e_{Si_2H_4} = k_9 n_{SiH_2} n_{SiH_4} / (k_{23} n_{H_2} + k_{13} n_{SiH_4})$ [3]. If it were not for reaction R13 that diverts part of the silicon atoms to higher silanes, reactions R23 and R9 would compensate one another and the only mechanism for silylyl to escape from the discharge zone would be its diffusion to the surface for deposition and pumping out. Given the above considerations, we can derive the effective rate constant of chemical removal of silylyl from the discharge:

$$k_{eff} = k_9 k_{13} n_{SiH_4} / \left(k_{23} n_{H_2} + k_{13} n_{SiH_4}\right) \cong k_9 / \left(n_{H_2}/n_{SiH_4} + 1\right). \tag{2.22}$$

The last approximate equality is a consequence of $k_{13} \cong k_{23}$. Therefore, the behavior of silylyl can be described by the equations

$$-D_{SiH_2}\, d^2 n_{SiH_2} / dx^2 = 2k_2 n_e n_{SiH_4} - k_{ef} n_{SiH_2} n_{SiH_4},\ 0 < x < l \tag{2.23}$$

$$-D_{SiH_2}\, d^2 n_{SiH_2} / dx^2 = k_{15} n^2_{SiH_3} - k_{ef} n_{SiH_2} n_{SiH_4},\ l < x < L\ . \tag{2.24}$$

By solving these equations with corresponding boundary conditions, an analytical expression for the flux of silylyl (SiH_2) to the surface has been obtained, but, in view of its complexity, we do not present it here.

2.7. Simulation results

To validate the model we simulated the deposition process in a wide range of operating conditions and compared the simulation results with experimental data available.

Furthermore, we studied the influence of various controllable parameters on the processes occurring in a PECVD reactor. In our simulations, we paid special attention to parameters considered to be important for either adjusting or assessing the reactor performance, namely the influence of flow rate, reactor volume, silane dilution, substrate separation in remote plasma configuration, as well as the "dust" production.

2.7.1. Comparison with experiment

Comparison with experimental data in the literature is difficult, because the set of parameters describing the system available is far from complete. For this reason, we chose the results given in [4] for comparison. In this work, extensive information on the experimental conditions and results of numerical calculations are described.

The experimental installation was a chamber with a volume of 10 liter and contained two electrodes of radius 8 cm located 2.7 cm apart. For this configuration, the ratio of the reaction volume to the total volume of the chamber is $R_v = 0.054$ (for more details, see Section 2.7.5). The experiments were carried out with a mixture of silane and hydrogen in equal molar concentrations with a flow rate equal to 3.6 l/h under normal atmospheric conditions; the temperature in the reactor was 400 K. A program for computing parameters of the RF discharge between two plane-parallel electrodes was used to calculate the electron densities [5]. The main problem is to obtain a good estimate of the discharge power. In [4], from a comparison of the self-bias potential computed in simulations of argon plasma based on corresponding experiments, it was determined that the power directed to the discharge amounted to 50% of the total power. The same conclusion was made from a comparison of the calculated concentrations of H_2 and SiH_4 in the hydrogen–silane plasma with experimental data. Therefore, in calculations performed for the suggested model, we used a discharge power of 5 W, as has been proposed in [4].

Fig. 2.3 shows the dependence of the film growth rate on the discharge frequency at a constant pressure of 16 Pa in the reactor. As can be seen from this graph, the results are in good agreement with experimental data up to a frequency of ~ 30 MHz. At frequencies higher than ~ 30 MHz, the calculated curve tends to level off. The same tendency, although more gradual, was noted in the simulations reported in [4]. At the same time, in [4], the *experimental* dependence of the growth rate on the frequency was shown to be approximately linear. This discrepancy between experiment and theory seems to be persistent and is not well understood.

From the calculations of the partial pressures of molecular hydrogen and silane as functions of the discharge frequency given in Fig. 2.4, one can see that the data obtained using the approach developed in this study are in better agreement with experiment than the calculation results obtained in [4].

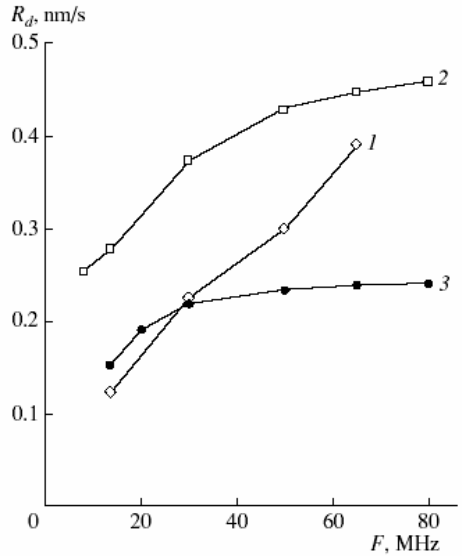

Fig. 2.3. Film growth rate as a function of discharge frequency at constant pressure in the chamber p = 16 Pa. (1) Experiment [4], (2) calculation [4], and (3) this work.

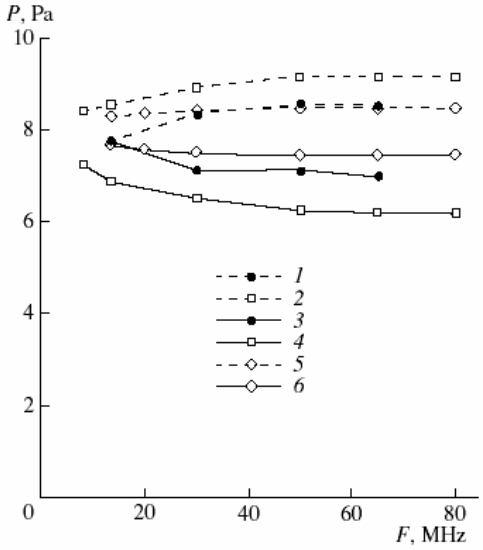

Fig. 2.4. Partial pressures of molecular hydrogen (dashed lines 1, 2, 5) and silane (solid lines 3, 4, 6) as a function of discharge frequency. Filled circles (1, 3): experiment [4]. Squares (2, 4): calculation [4]. Diamonds (5, 6): this work.

2.7.2. Specific features of chemical kinetics at low pressures

With the model described in this chapter, calculations of the processes are possible at low pressures, at which silane decomposition becomes noticeable and the concentration of molecular hydrogen can no longer be considered small. Below, we discuss in detail the qualitative differences of these low-pressure processes from those taking place at high pressures.

Dependence of the electron density in the discharge zone on the process parameters was described by a formula derived for the case of constant discharge power [3]

$$n_e\left(p_{SiH_4} l\right) = n_e^0 p_{SiH_4}^0 l^0 / p_{SiH_4} l, \tag{2.25}$$

where n_e^0 is the electron density under basic conditions, taken equal to $5 \cdot 10^8$ cm^{-3}.

This formula is true for pressures that are not very low, but it was used for the qualitative analysis in the entire range of pressures. For other key parameters of the problem, values characteristic of real experimental setups were chosen [1,2]: the temperature in the reaction chamber was taken equal to 520 K, the pressure was 0.25 Torr, and the inter-electrode distance was $l = L$ = 2.5 cm. Under these conditions, the reactor parameters corresponded to a characteristic pumping time of τ = 1s at a pressure of 1 Torr (for more details see Section 2.7.4). The calculations were carried out for a pressure range $0.02 < p < 1$ Torr. All the results given in this section refer to the case of pure silane as the carrier.

One of the main distinctions of the considered processes is a considerable rise in the concentration of atomic hydrogen with decreasing pressure. There are a number of reasons for this. First of all, as seen from formula (2.18), the concentration of atomic hydrogen in the particular case of homogeneous discharge is given by formula (2.26), i.e., it depends only on the electron density:

$$n_H = 2k_2 n_e / k_8 . \tag{2.26}$$

This formula is also in good agreement with the calculation results. At the same time, as seen from formulas (2.13), (2.14), and (2.25), the electron density and the constant k_2 rise rapidly with decreasing silane pressure, so that the concentration of atomic hydrogen increases by nearly five orders of magnitude as the pressure in the chamber decreases from 1.0 to 0.02 Torr and the relative silane concentration decreases to 0.3 as a result of its decomposition. The increase in atomic hydrogen concentration causes qualitative changes in various processes.

The behavior of other components with variations in pressure does not change compared with the description in [3], except for the fact that the concentration of Si_2H_6 drops at pressures below 0.1 Torr. The same effect is observed for Si_3H_8. This is due to a noticeable drop in silane concentration and the increase in atomic hydrogen concentration, the main reactants that determine the formation and decomposition of these components. The increase in the atomic hydrogen concentration also affects the balance and role of different reactions in silyl decomposition. Thus, at low pressures, an increase in the role of the decomposition process in the silyl balance is observed; at 0.02 Torr, it becomes dominant and prevails over deposition. Note, however, that this result is entirely a property of the model, because the use of formula (2.25) at very low pressures gives values of the electron density that are too high.

At pressures below about 0.08 Torr in silyl decomposition, the reaction $SiH_4 + Si_3H_8 \rightarrow Si_4H_9 + H_2$ gives way as the dominant process to reaction $SiH_3 + SiH_3 \rightarrow SiH_4 + SiH_2$; and at pressures of about 0.02 Torr, to the reaction between silyl and atomic hydrogen, which begins to make a noticeable contribution to the production of silyl. As before, silyl formation is completely dominated by the reaction between silane and atomic hydrogen.

Contributions of individual reactions to the silylyl balance remain largely unchanged, but its production at low pressures increases so much that most of the silylyl is deposited instead of being decomposed. Because of all these changes, the contribution of silylyl to film growth, which, with decreasing pressure, increases at a greater rate than that of silyl, becomes dominant at a pressure of 0.02 Torr. This should cause appreciable modifications in the film structure.

Taking into account silane decomposition at low pressures revealed further details of the division [3] of all components into three groups: stationary, nonstationary, and quasi-stationary. It was found that SiH can be considered strictly stationary only at high pressures. In addition, at high pressures, stationary components also include silylyl, the balance of which is maintained by two reactions with silane: $SiH_4 + e \rightarrow SiH_2 + 2H + e$ and $SiH_4 + SiH_2 \rightarrow Si_2H_6^*$, with the latter reaction keeping the concentrations of $Si_2H_6^*$ and Si_2H_4 (which is produced via decomposition of $Si_2H_6^*$) stationary. At low pressures, these last two components go over to the quasi-stationary group because of the appreciable

decomposition of silane, resulting in an increase in electron density and reaction rate constants. This is especially noticeable in the behavior of atomic hydrogen, whose concentration at high pressure is stationary and adequately described by formula (2.26). At low pressures, the deviation from stationarity caused by these processes makes atomic hydrogen non-stationary and appreciable accumulation of this component in the reaction chamber begins. Other parts of this classification remain qualitatively unchanged (see details in [3]).

2.7.3. Influence of diffusion coefficients

The use of formula (2.9) in calculating the diffusion coefficients does not significantly change the main results (such as the growth rate and film composition) compared with calculations in which these coefficients were assumed to be equal to the coefficients of the respective components in silane, as was done in [3]. This result appears to be quite evident at high pressures, where the concentration of molecular hydrogen is rather low and the diffusion coefficients calculated by formula (2.9) are close to the corresponding ambipolar coefficients. However, at low pressures, these values are distinctly different.

This fact suggests that the concentration profiles of the depositing components adjust in such a way as to maintain the production–deposition balance, irrespective of the particular values of the diffusion coefficients (the rate of chemical decomposition of silyl and silylyl at low pressures is small).

For a more detailed investigation of this issue, calculations using the above approach were carried out for a mixture of silane and molecular hydrogen at equal partial pressures and constant electron density $5 \cdot 10^8$ cm^{-3}. In this case, the influence of the diffusion coefficients is more pronounced. For the same purpose, a simplified formula was used to calculate reaction rate constants as functions of pressure [3]:

$$\frac{k_r}{k_r^0} = \left(\frac{l^0 p^0}{l_p} \right)^{2\epsilon_r/\epsilon_i} . \qquad (2.27)$$

Under these conditions, the diffusion coefficients calculated by Wilke's formula differ from the ambipolar diffusion coefficients by a factor of 1.6–1.7. Still, at low pressures where the silyl–silylyl balance is dominated by deposition, the fluxes of these components to the substrate practically coincide in the two cases, despite the distinctly different concentration profiles (see Fig. 2.5). At high pressures, silylyl is spent mainly through reactions in the bulk and the values of fluxes obtained with the use of constant ambipolar diffusion coefficients are somewhat less than those given by Wilke's formula; however, this difference is a mere 10% for silyl and 20% for silylyl, which is much less than the difference in the coefficients, and the contribution of silylyl to film growth under these pressures is insignificant.

To check this, a series of calculations was carried out for varying values of the diffusion coefficients. In one of these, the diffusion coefficient for silyl was assumed to be twice as large. The film growth rate was almost unchanged, although at a pressure of 1 Torr, the silyl concentration dropped by a factor of 1.5.

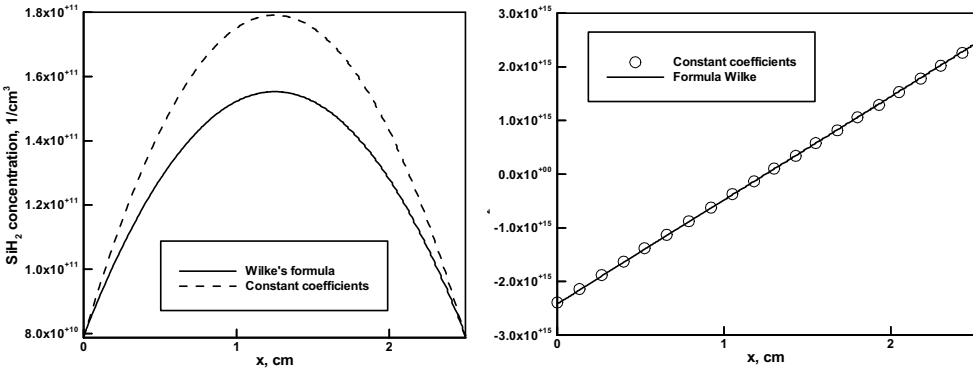

Fig. 2.5. SiH_2 concentration profiles (left) and SiH_2 fluxes (right) obtained with constant coefficients and using Wilke's formula. Pressure is 0.02 Torr

This fact is explained as follows. Because the dominant contribution to film growth comes from the flux of silyl, the growth rate can be analyzed using expression (2.20). At $d = 0$, this expression is significantly simplified, reducing to $\Gamma_{SiH_3} = 2k_2 n_e n_{SiH_4} L_3 \tanh(L/2L_3)$. For real values of the diffusion coefficient, $L/2L_3 < 0.7$ throughout the range of pressures studied and, therefore, the dependence of Γ_{SiH_3} on L_3 is weak. An increase in the diffusion coefficient only reduces the dependence of the flux of silyl on its value. Thus, silyl deposition is virtually unaffected by diffusion processes.

A similar result was also obtained for silylyl. The twofold increase in the silylyl diffusion coefficient did not produce any significant changes. At low pressures, the silylyl concentration decreased, but the modified profiles ensured exactly the same value of its flux. At higher pressures, the silylyl balance is completely controlled by chemical reactions; therefore, its concentration (as well as concentrations of all other components) remained the same, but the flux increased somewhat (by 37% at p = 1 Torr). However, at this pressure, the contribution from SiH_2 to film growth is quite small and cannot change the final result.

It can be concluded from the above analyses that further refining the diffusion transport description will not significantly change the results, especially in case of pure silane plasma.

2.7.4. Effect of the flow rate

The flow rate of the mixture through the working reactor volume is one of the important factors affecting the film growth parameters, and, at the same time, it can be easily varied. In [3], an approach that allows one to take into account the effect of the flow rate using a simple one-dimensional model was suggested. In this approach, the initial steady-state problem is replaced with a transient problem solved for a time period τ equal to the characteristic time of transit of the mixture in the reactor working volume. Decomposition of a considerable part of silane occurring at low flow rates and a significant increase in the molecular hydrogen concentration render the model suggested in [3] inapplicable for studying the role of the flow rate in a relatively wide range of this parameter.

Using the model presented in this study, the effect of the flow rate has been analyzed for the example of pure silane for τ ranging from 0.13 to 2.6 s, which, at a pressure of 0.25 Torr, corresponds to a change in the chamber volume from 1 to 20 l for the fixed flow rate of silane of 5 l/h at atmospheric pressure. Values of the other parameters were the same as in the previous sections, and the electron density was calculated by formula (2.25).

As in [3], variation of the flow rate was found to affect, first of all, the concentration of Si_2H_6: it increased by an order of magnitude as the flow rate was reduced by the same factor. At the same time, the concentration of Si_3H_8 increased by a factor of about 5. In the considered range of τ, the variation of the flow rate causes relatively small variation of the film characteristics. With a decreasing flow rate, the film growth rate increased by 30%. This was due to an increase in both the electron density and the reaction rate constants with a decreasing partial concentration of silane. The relative contribution of silylyl increased by about the same amount. This was caused by an increase in the concentration of molecular hydrogen and, subsequently, a greater contribution to the recovery of the silylyl concentration from the cyclic reaction $SiH_4 + SiH_2 \rightarrow Si_2H_6^* \rightarrow Si_2H_4 + H_2 \rightarrow SiH_4 + SiH_2$.

2.7.5. Effect of chamber volume

The problem considered above is closely related to the effect of the ratio of the reaction volume to the entire chamber volume, because circulation of the components throughout the volume can change the course of the processes.

To investigate this aspect in a one-dimensional case, the following approach was suggested: the area under study was expanded by adding a region R such that the ratio R_v would have been equal to the total chamber volume. The calculations for a fixed parameter τ and variable R_v gave estimates of the effect of circulation. The results described below were obtained for a total chamber volume of 2 l and $\tau = 0.26$ s; other parameters were the same as before.

Changing the parameter R_v from 1 to 0.2 resulted in an insignificant (about 25%) increase in the rates of film growth and silyl deposition. This increase was caused by increased concentrations of silane and silyl in the reaction volume because of the influx of SiH4 from the chamber volume. At the same time, silylyl deposition remained nearly constant, because some increase in its production due to the reaction of silylyl decomposition (R15) was offset by reaction $SiH_4 + SiH_2$ and deposition occurs only from a thin near-wall layer, where the concentration of silyl is low. Some distinctive features of these processes are illustrated in Fig. 2.6-Fig. 2.8.

In Fig. 2.6, profiles of typical representatives of the three classes of components are shown: non-depositing and slowly reacting (H_2), non-depositing and rapidly reacting (H), and depositing and rapidly reacting (SiH_2). It is seen that the concentrations of the latter two components in the reaction volume are practically independent of the chamber volume. They are determined by reactions proceeding in the discharge zone, and circulation has little effect on them. The concentration of molecular hydrogen, on the contrary, is constant throughout the chamber volume and is appreciably reduced by circulation.

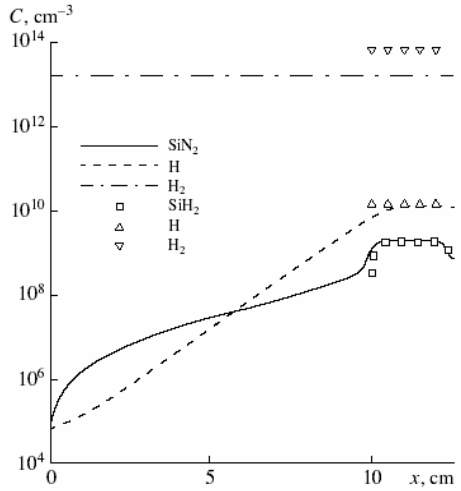

Fig. 2.6. Concentration profiles of silylyl and molecular and atomic hydrogen at different values of the ratio of reaction volume to the total chamber volume Rv̧ equal to 0.2 (curves) and 1 (dots)

The small diffusion-reaction length for silylyl with respect to the chamber dimensions is the reason for the weak influence of the chamber volume on the balance and flows of this radical (Fig. 2.7, Fig. 2.8). Only some increase in its production due to a higher silane concentration can be noted; this increase is compensated by its more intensive (for the same reason) decomposition, so that flows onto the substrate turn out to be about the same.

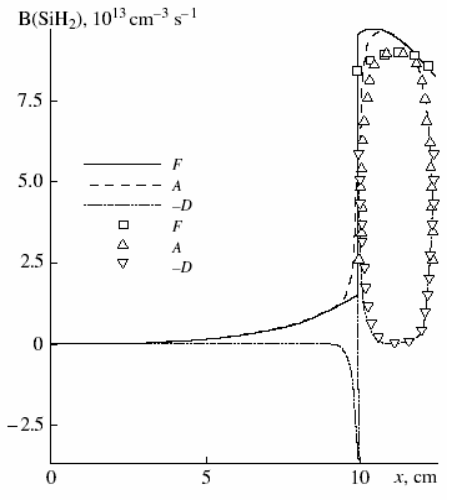

Fig. 2.7. Silylyl balance at different values of the ratio of reaction volume to the total chamber volume R_v. F, production; A, decomposition; D, diffusion; R_v = 0.2 (curves) and 1 (dots).

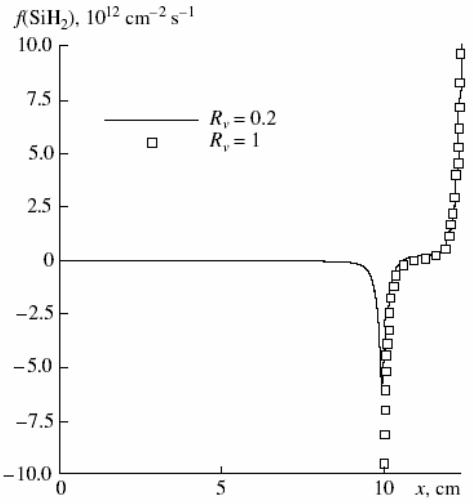

Fig. 2.8. Silylyl fluxes at different values of the ratio of the reaction volume to the total chamber volume R_v.

2.7.6. Effect of diluting silane with molecular hydrogen

In real experiments, a mixture of silane and molecular hydrogen is widely used. To evaluate the effect of silane dilution, calculations have been carried out for a silane content in this mixture varying from 100 to 20%, the other parameters having the same values as before. The electron density was determined using an RF discharge model [5]. Calculations for a discharge power of 0.025 W/cm^2 have shown that, in these conditions, the average electron density rises nearly linearly from $4.3 \cdot 10^8$ to $6.7 \cdot 10^8$ cm^{-3} as the silane content in the mixture is reduced.

As the silane content is reduced at constant pressure, the diffusion coefficients of the components, with the exception of H_2, increase by a factor of 2–3. Variation of the concentrations of all reaction products under these conditions is shown in Fig. 2.9. The film growth rate rises, and the relative contribution of silylyl to the overall deposition becomes larger (Fig. 2.10). The growth rate rises, despite falling silane concentration, because of an increase in the total production of depositing components due to higher rate constants of reactions initiated by electron impact (see expressions (2.13) and (2.14)) and increased electron density. In addition, the net result of lowering the concentration and the simultaneous increase in the diffusion coefficients is that the greater part of the produced silyl is deposited; this is true for other depositing components, except Si_2H_3 and Si_2H_4, which are effectively decomposed by molecular hydrogen. The behavior of silylyl is explained by the fact that with an increasing concentration of H_2 and a decreasing concentration of silane, the fraction of silylyl being deposited rises significantly. At the same time, the intensity of the above-mentioned cyclic reaction rises, leading to the recovery of the SiH_2 concentration.

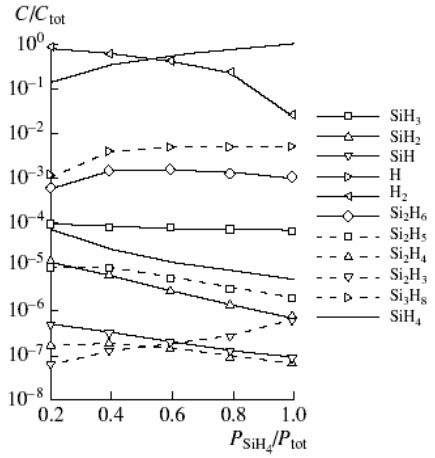

Fig. 2.9. Concentrations of components versus the silane fraction in the initial silane–hydrogen mixture at constant pressure.

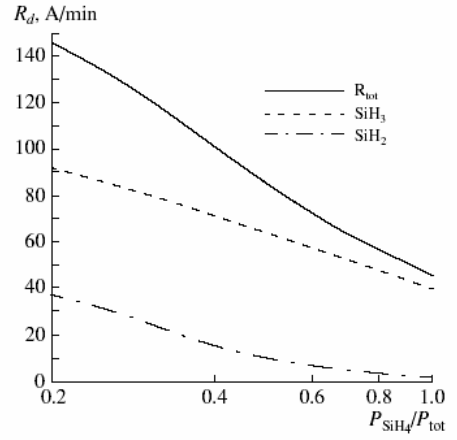

Fig. 2.10. Film growth rate and contributions of silyl and silylyl to it versus the fraction of silane in the initial silane–hydrogen mixture at constant pressure.

Also worth noting is the considerable reduction in the Si_3H_8 concentration with dilution (Fig. 2.9). The reason is that alongside the drop in production by the reaction $SiH_4 + Si_2H_4$, it is decomposed via the reaction with atomic hydrogen, whose concentration rises at a high rate. The result is a drastic drop in Si_4H_9 production, and the greater part of the silicon produced in the reaction is deposited.

2.7.7. Specific features of a triode system

All the results described above were obtained for a diode system in which the discharge zone is located between two electrodes, one of which serves as a substrate for the growing film (schematically shown in Fig. 1.1). One alternative technology is a so-called triode system, in which the discharge zone is separated from the substrate (see Section 2.1).

In order to investigate the effect of the separation of electrodes from the substrate, calculations of film growth from a pure silane plasma were carried out for the same problem parameters as previously used (with the exception of parameter L = 5 cm, with parameter l/L varying from 0.4 to 1). The average electron densities calculated with the RF discharge model [5] were varied from $6.8 \cdot 10^8$ to $4.9 \cdot 10^8$ cm^{-3}. The simulation results obtained using the above analytical expressions for the silyl flux (2.20) and the concentration profile of atomic hydrogen (2.18), (2.19) are in good agreement with numerical simulation results, as seen in Fig. 2.11 and Fig. 2.12, respectively.

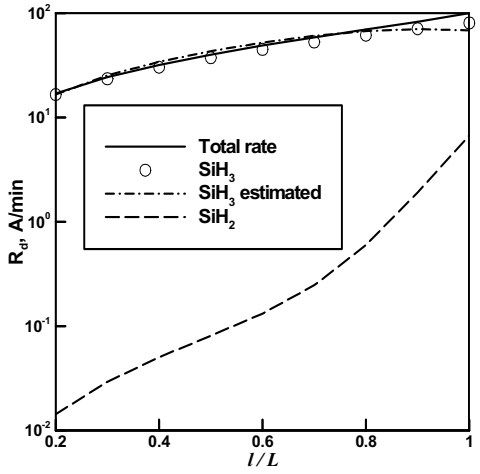

Fig. 2.11. Film growth rate and contributions of silyl and silylyl versus the ratio of discharge zone to the total reactor zone. Numerical and analytical solutions (formula (2.20)).

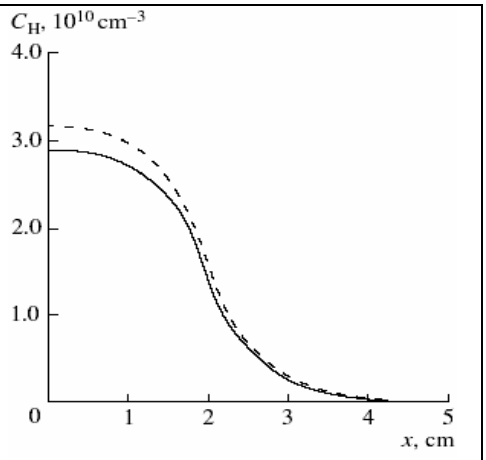

Fig. 2.12 Atomic hydrogen profiles for the triode reactor system (l/L = 0.4): solid curve, analytical solution; dashed curve, numerical solution.

As a result of varying the parameter l/L in the range specified above, the film growth rate (at a constant discharge power) decreased by only half. The cause of the slow decrease in the growth rate with increasing separation between the electrode and the substrate is the increase in electron densities and rate constants of reactions initiated by electron impact as the inter-electrode separation l is reduced, which partially compensates decomposition of

silicon-containing components outside the discharge zone. In addition, a drastic reduction in the contribution to the film growth from silylyl should be noted, starting as soon as the electrode is moved away from the substrate (Fig. 2.11).

This is especially remarkable in view of the fact that at the same time, its concentration and total production are rising. Two main reasons for this effect can be indicated. The first is that the diffusion-reaction length of silylyl is much less compared with that of silyl; therefore, the bulk decomposition of silylyl is more efficient. The second reason is their very different production mechanisms. The major source of silyl is the reaction between silane and atomic hydrogen, which, as seen in Fig. 2.12, diffuses quite intensively beyond the discharge zone.

On the other hand, the main contribution to silylyl production comes from the reaction between silane molecules themselves; therefore, production of SiH_2 outside the discharge is small.

One should pay attention to the rapid diminishing of high silane production that leads to the deposition of greater part of produced silicon (see Fig. 2.13).

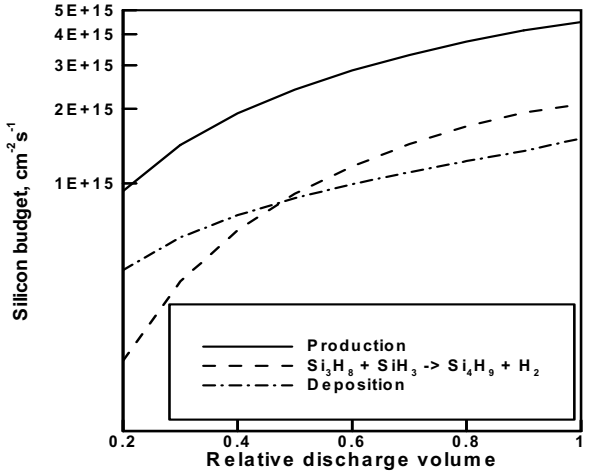

Fig. 2.13. Silicon budget.

2.7.8. Analysis of the diffusion-reaction lengths

Analysis of the flow in typical PECVD reactors showed that diffusion is the prevalent transport mechanism in the discharge volume between the parallel plate electrodes. To analyze the different behaviour of the particles, a diffusion-reaction length can be introduced [3] that characterizes the distance a particle Si_mH_n will diffuse over before undergoing chemical reaction:

$$L_{m,n} = (D_{m,n}/\nu_{m,n})^{1/2} \quad (2.28)$$

Here $D_{m,n}$ is the effective diffusion coefficient and $\nu_{m,n}$ is the removal rate of the *i*th species due to chemical reactions. Analysing diffusion-reaction lengths for different components of the mixture, one can get an idea of their spatial distribution; clarify their effect on the

composition of the mixture and separate out the boundary region, which gives a major contribution to the film growth. The value of this diffusion-reaction length determines the shape of the concentration profile between the electrodes: for low values the concentrations take the equilibrium values at all points in the chamber, falling abruptly to zero at the wall if the particles stick to the surface, or stay at equilibrium if they do not deposit. At high values of diffusion-reaction length the concentration distribution in space is smoothed out and weakly depends on local chemical reactions.

Fig. 2.14 shows the pressure dependence of diffusion-reaction lengths in the range of 0.15–1.00 Torr near two opposite electrodes (walls) maintained at temperatures T_w = (a) 300 and (b) 520 K, respectively [19], for the set of reactions listed in Table 2-3.

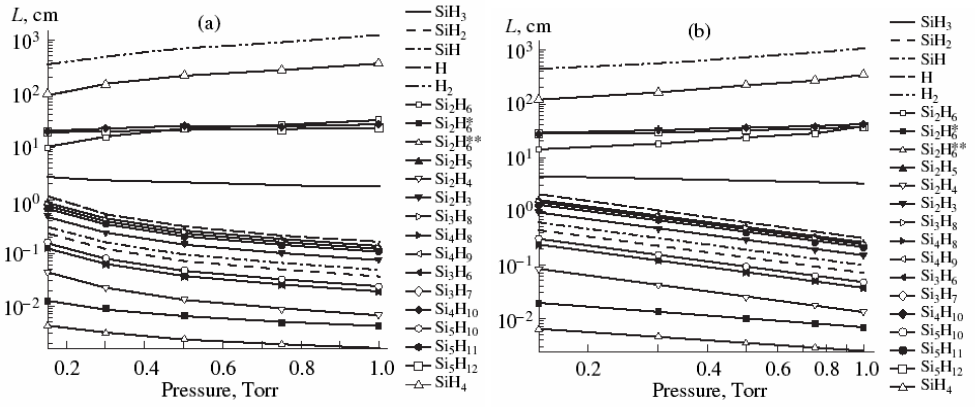

Fig. 2.14 Diffusion-reaction lengths vs. pressure at the (a) hot (Tw = 520 K) and (b) cold (Tw = 300 K) walls.

As we can see, all the components fall into three groups according to their diffusion-reaction lengths and the pressure dependences of these lengths. Molecules (particles with saturated bonds) fall into the first group. This group features relatively large diffusion-reaction lengths and their weak increase with pressure. For the species from this group, the reactions governing the removal rate $\nu_{m,n}$ are reactions with Si_2H_4 (molecular hydrogen); reactions with atomic hydrogen (and Si_2H_6); reaction with SiH_3 and at lower pressures with SiH_2 (species like Si_nH_{2n+2} with $n > 2$). Silyl (SiH_3) falls into the second group, because its diffusion-reaction length, first, differs from the corresponding values for the rest of the components and, second, slightly decreases with increasing pressure. This stems from the fact that silyl leaves the system not only through the reaction with itself but also through the reaction with silane. Since the effect of the latter reaction increases with pressure (when the silane concentration evidently rises), the removal rate turns out to be a function decreasing more slowly than $1/p$ (this is true for the pressure range considered; at higher pressures, it starts to increase). Accordingly, $L_{1,3}$ drops. The rest of the radicals fall into the third group. They feature relatively short diffusion-reaction lengths that decrease with increasing pressure. This is because the removal rate of these species is proportional to the concentrations of SiH_4 or H_2, which in turn are proportional to the pressure in the case at

hand and considerably exceed the concentrations of the other species. Thus, the corresponding lengths become inversely proportional to pressure.

The results of the film growth process were analyzed in [19]. A short summary of the key conclusions is presented here. Fig. 2.15 shows that the contribution from Si_2H_5 to the film growth is of the same order of magnitude as that from SiH_2. Our interest in the amount of the silylene deposit is explained by the fact that this radical is frequently viewed as the main cause for film degradation [3]. However, the other species are deposited in comparable (to silylene) amounts, making us attribute to them the same adverse effect. Analysis of the chemical reactions in the reactor suggests that a high effect of Si_2H_5 is associated with its relatively high diffusion-reaction length, which is approximately four times higher than that of SiH_2. In other words, the area of Si_2H_5 deposition is larger than that of silylene. The contribution from Si_3H_7 is appreciable; it is only 2.5 times lower than the contribution from Si_2H_5. A high efficiency of Si_3H_7 is related to its high concentration: the reaction of the Si_2H_4 radical with silane yields a high concentration of Si_3H_8 (R40: $Si_2H_4 + SiH_4 \rightarrow Si_3H_8$), which in turn produces Si_3H_7 in the reaction with silyl (R45: $Si_3H_8 + SiH_3 \rightarrow Si_3H_7 + SiH_4$). Thus, the noticeable contribution of Si_3H_7 to the film growth is explained by two factors: a high concentration of silane and a high reactivity of the Si_2H_4 radical. The diffusion-reaction length of Si_3H_7, as well as of Si_2H_5, is four times as large as that of SiH_2 and, accordingly, causes the same consequences.

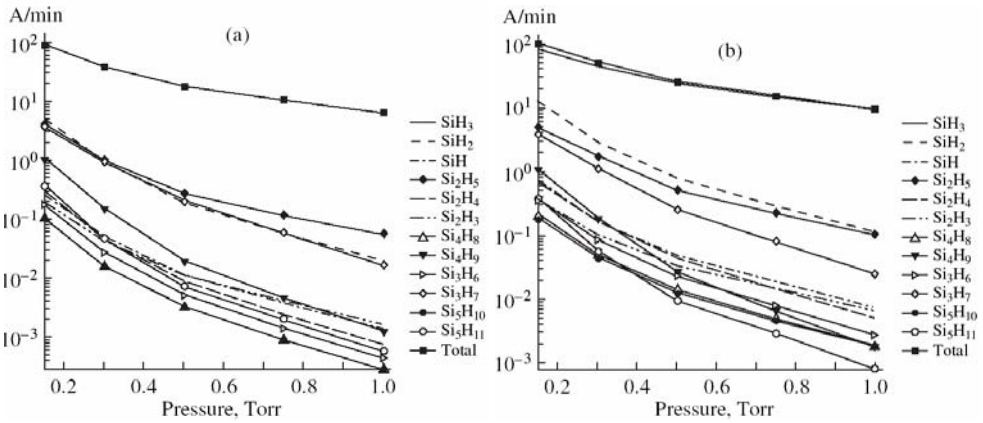

Fig. 2.15 Deposition rates of different components vs. pressure at the (a) hot (Tw = 520 K) and (b) cold (Tw = 300 K) walls.

Table 2-3. List of chemical reactions and reaction constants

Reaction no.	Reaction	K (cm^3/s)	Reaction no.	Reaction	K (cm^3/s)
R1	$SiH_4 + e \longrightarrow SiH_3 + H + e$	3.00(–11)[a, b]	R39	$Si_2H_4 + H_2 \longrightarrow Si_2H_6$	5.33(–13)
R2	$SiH_4 + e \longrightarrow SiH_2 + 2H + e$	1.50(–10)[b]	R40	$Si_2H_4 + SiH_4 \longrightarrow Si_3H_6 + H_2$	1.00(–11)[f]
R3	$SiH_4 + e \longrightarrow SiH + H + H_2 + e$	9.34(–12)[b]	R41	$Si_2H_4 + SiH_4 \longrightarrow Si_3H_8$	1.00(–10)
R4	$SiH_4 + e \longrightarrow SiH_2 + H_2 + e$	7.19(–12)[b]	R42	$Si_2H_3 + H_2 \longrightarrow Si_2H_5$	1.70(–12)
R5	$H_2 + e \longrightarrow 2H + e$	4.49(–12)[b]	R43	$Si_3H_8 + H \longrightarrow Si_2H_5 + SiH_4$	1.11(–12)[g]
R6	$Si_2H_6 + e \longrightarrow SiH_3 + SiH_2 + H_2 + e$	3.72(–10)[b]	R44	$Si_3H_8 + H \longrightarrow Si_2H_6 + SiH_3$	1.11(–12)[c]
R7	$Si_2H_6 + e \longrightarrow Si_2H_4 + 2H + e$	3.70(–11)[b]	R45	$Si_3H_8 + H \longrightarrow Si_3H_7 + H_2$	2.16(–12)[c]
R8	$SiH_4 + H \longrightarrow SiH_3 + H_2$	2.67(–12)[c]	R46	$Si_3H_8 + SiH_3 \longrightarrow Si_3H_7 + SiH_4$	2.49(–12)[c]
R9	$SiH_4 + SiH_3 \longrightarrow Si_2H_5 + H_2$	1.78(–15)	R47	$Si_3H_8 + SiH_2 \longrightarrow Si_4H_{10}$	1.20(–10)[c]
R10	$SiH_4 + SiH_2 \longrightarrow Si_2H_6^*$	1.00(–11)	R48	$Si_3H_8 + SiH \longrightarrow Si_4H_9$	1.00(–11)
R11	$SiH_4 + SiH \longrightarrow Si_2H_3 + H_2$	1.70(–12)	R49	$Si_3H_8 + Si_2H_5 \longrightarrow Si_3H_7 + Si_2H_6$	2.49(–12)[c]
R12	$SiH_4 + SiH \longrightarrow Si_2H_5$	2.50(–12)	R50	$Si_3H_8 + Si_2H_4 \longrightarrow Si_5H_{12}$	1.00(–10)[d]
R13	$SiH_3 + H \longrightarrow SiH_2 + H_2$	1.00(–10)	R51	$Si_3H_7 + H \longrightarrow Si_3H_8$	1.00(–11)
R14	$SiH_3 + SiH_3 \longrightarrow SiH_4 + SiH_2$	1.50(–10)	R52	$Si_3H_7 + SiH_4 \longrightarrow Si_3H_8 + SiH_3$	5.00(–13)[h]
R15	$SiH_3 + SiH_3 \longrightarrow Si_2$	1.00(–11)	R53	$Si_3H_7 + SiH_3 \longrightarrow Si_3H_6 + SiH_4$	1.00(–10)[i]
R16	$SiH_3 + SiH_2 \longrightarrow Si_2H_5$	3.77(–13)	R54	$Si_3H_7 + SiH_3 \longrightarrow Si_4H_{10}$	5.50(–11)[j]
R17	$SiH_2 + H \longrightarrow SiH + H_2$	7.96(–13)	R55	$Si_3H_7 + SiH_2 \longrightarrow Si_4H_9$	1.00(–11)
R18	$SiH_2 + H \longrightarrow SiH_3$	1.11(–12)	R56	$Si_3H_6 + SiH_4 \longrightarrow Si_4H_8 + H_2$	1.00(–11)[f]
R19	$SiH_2 + H_2 \longrightarrow SiH_4$	2.00(–13)	R57	$Si_3H_6 + SiH_4 \longrightarrow Si_3H_8$	1.00(–11)[k]
R20	$SiH_2 + SiH \longrightarrow Si_2H_3$	7.22(–13)	R58	$Si_3H_6 + SiH_3 \longrightarrow Si_4H_9$	2.00(–11)
R21	$SiH + H_2 \longrightarrow SiH_3$	1.98(–12)	R60	$Si_4H_{10} + SiH_3 \longrightarrow Si_4H_9 + SiH_4$	2.49(–12)[m]
R22	$Si_2H_6 + H \longrightarrow SiH_4 + SiH_3$	1.11(–12)[c]	R61	$Si_4H_{10} + SiH_2 \longrightarrow Si_5H_{12}$	1.20(–10)[n]
R23	$Si_2H_6 + H \longrightarrow Si_2H_5 + H_2$	1.20(–10)[c]	R62	$Si_4H_{10} + SiH \longrightarrow Si_5H_{11}$	1.00(–11)
R24	$Si_2H_6 + SiH_3 \longrightarrow Si_2H_5 + SiH_4$	1.00(–12)[c]	R63	$Si_4H_9 + H \longrightarrow Si_4H_{10}$	1.00(–11)
R25	$Si_2H_6 + SiH_2 \longrightarrow Si_3H_8$	1.20(–10)	R64	$Si_4H_9 + SiH_4 \longrightarrow Si_4H_{10} + SiH_3$	5.00(–13)[h]
R26	$Si_2H_6 + SiH \longrightarrow Si_3H_7$	1.00(–11)	R65	$Si_4H_9 + SiH_3 \longrightarrow Si_4H_8 + SiH_4$	1.00(–10)[i]
R27	$Si_2H_6 + Si_2H_4 \longrightarrow Si_4H_{10}$	1.00(–10)[d]	R66	$Si_4H_9 + SiH_3 \longrightarrow Si_5H_{12}$	5.50(–11)[j]
R28	$Si_2H_6^* + M^e \longrightarrow Si_2H_6 + M$	1.00(–10)	R67	$Si_4H_9 + SiH_2 \longrightarrow Si_5H_{11}$	1.20(–10)[n]
R29	$Si_2H_6^* \longrightarrow Si_2H_4 + H_2$	5.00(6) s^{-1}	R68	$Si_4H_8 + SiH_4 \longrightarrow Si_5H_{10} + H_2$	1.00(–11)[f]
R30	$Si_2H_6^{**} \longrightarrow SiH_4 + SiH_2$	2.30(7) s^{-1}	R69	$Si_4H_8 + SiH_4 \longrightarrow Si_5H_2$	1.00(–11)[k]
R31	$Si_2H_6^{**} \longrightarrow Si_2H_4 + H_2$	2.30(7) s^{-1}	R70	$Si_4H_8 + SiH_3 \longrightarrow Si_5H_{11}$	2.00(–11)
R32	$Si_2H_6^{**} + M^e \longrightarrow Si_2H_6 + M$	2.00(–10)	R71	$Si_5H_{12} + H \longrightarrow Si_5H_{11} + H_2$	2.16(–12)[l]
R33	$Si_2H_5 + H \longrightarrow Si_2H_4 + H_2$	1.00(–10)	R72	$Si_5H_{12} + SiH_3 \longrightarrow Si_5H_{11} + SiH_4$	2.49(–12)[m]
R34	$Si_2H_5 + SiH_4 \longrightarrow Si_2H_6 + SiH_3$	5.00(–13)	R73	$Si_5H_{12} + SiH_2 \longrightarrow Si_6H_{14}$	1.20(–10)[n]
R35	$Si_2H_5 + SiH_3 \longrightarrow Si_2H_4 + SiH_4$	1.00(–10)	R74	$Si_5H_{11} + H \longrightarrow Si_5H_{12}$	1.00(–11)
R36	$Si_2H_5 + SiH_3 \longrightarrow Si_3H_8$	5.50(–11)[c]	R75	$Si_5H_{11} + SiH_4 \longrightarrow Si_5H_{12} + SiH_3$	5.00(–13)[h]
R37	$Si_2H_5 + Si_2H_5 \longrightarrow Si_4H_{10}$	1.00(–11)	R76	$Si_5H_{11} + SiH_3 \longrightarrow Si_5H_{10} + SiH_4$	1.00(–10)[i]
R38	$Si_2H_4 + H_2 \longrightarrow SiH_4 + SiH_2$	1.00(–10)	R77	$Si_5H_{10} + SiH_4 \longrightarrow Si_6H_{14}$	1.00(–11)[k]

Notes: *a* 3.00(–11) = 3.00 . 10–11.

b Data for electron-impact reaction rates are given for the same reference conditions as in Table 2-2.

c The values of the constants are taken from [13].

d The values of the constants are taken by analogy with reaction R41 from [16].

e *M* is partial particle (collision partner).

f Reactions are proposed in [15].

The values of the constants were taken by analogy with:

g Reactions R22 and R44 in [13].

h Reaction R34 in [3].

i Reaction R35 in [16].

j Reaction R36 in [13].

k Reaction $SiH_2 + SiH_4$ Si_2H_6 taken from [13].

l Reaction R45 in [13].
m Reaction R46 in [13].
n Reaction R47 in [13].

2.8. Conclusions

In this work, numerical investigations of the growth of hydrogenated amorphous silicon films have been carried out under various conditions in the growth chamber.

Comparison with experimental data has demonstrated the ability of the model to predict the film growth rate and concentrations of individual components with reasonable accuracy.

It has been shown that the widely used technique of diluting silane with molecular hydrogen both increases the growth rate and reduces production of higher silanes, making this technology more economical and ecologically clean. Moreover, dilution increases the contribution of silylyl to film growth, appreciably affecting its properties.

Analysis of a widely used reactor system has been carried out. Numerical simulation has shown that the effective decomposition of silylyl outside the discharge zone reduces its contribution to film growth as the substrate is displaced away from the discharge.

The analytical expressions obtained for silyl and silylyl fluxes and for the profile of atomic hydrogen closely approximate the results of numerical computations and can be used for making the corresponding estimations.

In the next chapter we investigate the influence of flow on the deposition process in 2D and 3D geometries of a reactor chamber.

2.9. References

1. O. A. Golikova, Sov. Phys. Semicond. 25, 915 (1991).
2. M. J. Kushner, J. Appl. Phys. 63, 2532 (1988).
3. Yu. E. Gorbachev, M. A. Zatevakhin, and I. D. Kaganovich. Tech. Phys. 41, 1247 (1996)
4. G. J. Nienhuis, W. J. Goedheer, et al., J. Appl. Phys. 82, 2060 (1997).
5. V. A. Schweigert, M. I. Zhilyaev, I. V. Schweigert, Applied Mechanics and Technical Physics. 35 (1), 13 (1994).
6. C. R. Wilke, Chem. Eng. Prog. 46 (2), 95 (1950).
7. J. O. Hirschfelder, C. F. Curtiss, and R. B. Bird, Molecular Theory of Gases and Liquids (Wiley, New York, 1954; Inostrannaya Literatura, Moscow, 1961).
8. P. Ginzburg, Friction and Heat Transfer in Moving Gas Mixtures (Leningrad Univ., Leningrad, 1975).
9. J. Perrin and O. Leroy, Contrib. Plasma Phys. 36 (3), 3 (1996).
10. N. Itabashi, K. Kamo, and N. Nishawaki, Jpn. J. Appl. Phys. 28, 325 (1989).
11. J. Perrin, J. Phys. D 26, 1662 (1993).

12. Yu.E. Gorbachev, M.A. Zatevakhin, V.V. Krzhizhanovskaya, V. A. Shveigert. Special Features of the Growth of Hydrogenated Amorphous Silicon in PECVD Reactors. Technical Physics, Vol. 45, N 8, pp. 1032-1041. Publ.: MAIK Nauka/Interperiodika 2000
13. Yu.E. Gorbachev, M.A. Zatevakhin, V.V. Krzhizhanovskaya. Influence of Silane Dilution with Hydrogen and Inert Gases on the Dynamics of Amorphous Hydrogenated Silicon Films Growth in PECVD Reactors. Proceedings of the 2nd International Conference on Amorphous and Microcrystalline Semiconductors, St. Petersburg, Russia, 2000
14. Y.E. Gorbachev, M.A. Zatevakhin, V.V. Krzhizhanovskaya. Hydrogenated Amorphous Silicon Film Growth in Remote PECVD. Proceedings of the All-Russian Symposium on Amorphous and Microcrystalline Semiconductors, St. Petersburg, Russia, 5-9 July 1998, p.24
15. Yu.E. Gorbachev, M.A. Zatevakhin, V.V. Krzhizhanovskaya. Simulation of Amorphous Hydrogenated Silicon Plasma Enhanced Chemical Vapor Deposition in a Triode Reactor. Proceedings of the NATO workshop on Plasma Physics, St. Petersburg, Russia, 1997
16. Nienhuis, G.J., 1998, *Plasma models for silicon deposition*. PhD Thesis, Utrecht University.
17. Leroy, O., Gousset, G., Alves, L.L., Perrin, J., Jolly, J., 1998, Plasma Sources Sci. Technol., **7**, p. 348
18. K. De Bleecker, A. Bogaerts, R. Gijbels, W. Goedheer. Numerical investigation of particle formation mechanisms in silane discharges. PHYSICAL REVIEW E 69, 056409 (2004)
19. Yu.E. Gorbachev. Effect of Oligomers on the Growth of Amorphous Silicon Films in a PECVD Reactor. Technical Physics, 2006, Vol. 51, No. 6, pp. 733–739.
20. V. V. Krzhizhanovskaya, P.M.A. Sloot and Yu. E. Gorbachev. Grid-based Simulation of Industrial Thin-Film Production. Simulation: Transactions of the Society for Modeling and Simulation International, Special Issue on Applications of Parallel and Distributed Simulation in Industry, January 2005, V. 81, No. 1, pp. 77 - 85